Translated from *Uspekhi Khimii* **61** 356–383 (1992) U.D.C. 66.097 + 548.734 + 539.26

X-Ray diffraction study of carriers and deposited metallic catalysts

E M Moroz
Institute of Catalysis, Siberian Division of the Russian Academy of Sciences

ABSTRACT. The possibilities of applying some X-ray diffraction methods in the study of multicomponent highly disperse systems are examined. Such methods include the method based on the radial distribution of atoms (RDA), full-profile X-ray diffraction analysis (FPA), and the method involving the determination of substructural characteristics (MDSC). Examples of the determination of the structural and substructural characteristics of the most important catalyst carriers as well as deposited and non-deposited metallic catalysts are presented.

The bibliography includes 129 references.

Contents

I. Introduction 188
II. The possibilities of X-ray diffraciton methods in the study of multicomponent highly disperse systems 188
III. Structural and substructural characteristics of catalyst carriers 193
IV. Structural and substructural characteristics of deposited and non-deposited monometallic catalysts 196
V. Determination of the phase composition of deposited bimetallic catalysts 198
VI. Conclusion 200

I. Introduction

Despite the widescale use of X-ray diffraction methods in materials science, the application to the study of catalysts is mainly limited to qualitative and quantitative phase analyses of well crystallised coarsely disperse (crystallite size in the range 50–1000 Å) systems. In his concluding remarks in a well known monograph devoted to methods for the study of catalysts, Lambert[1] indicates eight criteria in terms of which the effectiveness of the method should be estimated: (1) the need to use centralised or local laboratory equipment; (2) speed of analysis; (3) the possibility of studying catalysts in the course of their operation or after use; (4) destructiveness or non-destructiveness of the method; (5) the universality of the method (sensitivity in relation to various chemical elements, suitability for the study of deposited and non-deposited catalysts); (6) the possibility of obtaining useful information in the presence of a large amount of contaminants formed during the operation of the catalyst; (7) cost; (8) thickness of the layer of the specimen investigated.

Evidently, from this standpoint, X-ray diffraction methods are entirely effective, but, since it is assumed that they yield information mainly about the structural and substructural characteristics of the bulk phase of the specimen, inadequate attention has been devoted to them. The authors of monographs in which the structural features of catalysts are discussed, for example, Lambert[1] and Anderson,[2] as a rule do not dwell on the X-ray diffraction methods for their investigation. At the Ist European Conference on Powder Diffraction held in March 1991 in Munich, a small number of experimental studies on highly disperse materials were presented,[3–9] only three of which[7–9] were devoted to the study of catalysts. Nevertheless, X-ray diffraction methods occupy a place among the series of physical methods for the study of catalysts, especially deposited catalysts, because they make it possible to obtain information simultaneously about the dispersity and phase composition of the active component and the carrier and about their structural characteristics and the degree of their interaction.

Examination of the usual parameters of the diffraction patterns of well crystallised substances, such as the positions, intensities, and form of the diffraction maxima, for the investigation of highly disperse multicomponent catalytic systems yields little information. Special X-ray diffraction methods for the investigation of highly disperse materials, based on the integral analysis of the curve for the X-ray scattering intensity, namely the method based on the radial distribution of atoms (RDA), the methods based on the determination of substructural characteristics (MDSC), and full-profile X-ray analysis (FPA), are being developed at the Institute of Catalysis of the Siberian Division of the USSR Academy of Sciences. This review deals with the fundamental possibilities of the methods developed and presents the results of their use in order to obtain structural and substructural characteristics of the principal catalysts carriers (aluminium oxides and carbon materials) as well as deposited and non-deposited metallic catalysts having different chemical compositions.

II. The possibilities of X-ray diffraction methods in the study of multicomponent highy disperse systems

1. Methods based on the radial distribution of atoms

Mainly liquids (solutions and liquid metals) and amorphous and vitreous materials have been studied experimentally by the RDA method (see, for example, Refs. 10–13). Procedures for the interpretation of data and for the analysis of errors of different kinds have been examined theoretically.[14–21] Catalysts have been studied by the RDA method in a number of investigations.[13,22–29] Many catalysts of different chemical composition have been investigated in the Laboratory of Structural Research Methods at the Institute of Catalysis of the Siberian Division of the USSR Academy of Sciences. This review presents the results of the investigation of catalyst carriers and metallic catalysts.

The X-ray diffraction RDA method is based on the relation between the atomic density (ρ) radial distribution function and the intensity of the coherent scattering of X-rays $i(s)$ in the diffraction experiment:

$$4\pi r^2\rho(r)=4\pi r^2\rho_0+(2r/\pi)\int_{s_{min}}^{s_{max}} i(s)s\sin(sr)ds, \quad (1)$$

$$\rho_0=\sum_{A=1}^{m}(n_AK_A)^2dL/M,$$

$$i(s)=\left[I(s)/N-\sum_{A=1}^{m}n_Af_A^2(s)\right]\Big/f_e^2(s),$$

where $\rho(r)$ is the spherically symmetrical atom distribution function, d the pyknometric density, L the Avogadro number, M the molecular weight, $I(s)$ the coherent component of the scattered diffraction beam, r the radius-vector of the inverse lattice, $\rho_0(r)$ the average density obtained for a completely random distribution of atoms, i.e. in the absence of interference, K the effective number of electrons, f_e the atomic unit factor, and N the number of atoms in the agglomeration.

In the case of binary systems, where the atoms of one system (phase) form separate groups since they are surrounded only by atoms of the same system, the formula has the following general form:[30,31]

$$\rho(r)=C_A\rho_{AA}(r)+C_B\rho_{BB}(r)+2C_AC_B\rho_{AB}, \quad (2)$$

where ρ_{AA}, ρ_{BB}, and ρ_{AB} are the partial RDA functions and C_A and C_B are the concentrations of individual phases.

It is useful to use Eqn. (2) instead of Eqn. (1) for comparable values of C_A and C_B. In deposited metallic catalysts, the concentration of the metal is low relative to the carrier ($C_B \ll C_A$), so that Eqn. 1 can be used.

For the calculation of the RDA curves, it is essential to have at one's disposal certain experimental and reference characteristics of the test substance. Such experimental data are (1) the set of data for the intensity of scattering by the specimen; (2) the set of data for the intensity of phonon scattering; (3) information about the thickness of the specimen and the pressing density (these quantities are important for systems consisting of light atoms); (4) chemical composition of the specimen ($n_A...n_m$) per molecule; (5) pyknometric density.

Data from reference sources include (1) the number of electrons in the atoms; (2) the absorption coefficients of the atoms for the given X-ray irradiation; (3) radiation wavelength; (4) atomic factors of the atoms. The RDA curves are plotted in terms of the variables $4\pi r^2\rho$ and $f(r)$, where r is expressed in Ångstroms and the electron density ρ in electron^2 Å^{-3}.

The quantitative parameters of the structure are the equilibrium interatomic distances (the values of r to which correspond the electron density peaks), the coordination numbers Z (determined from the areas of the coordination peaks), the averge quadratic atomic shifts (determined from the widths of the coordination peaks), as well as the distance over which the correlation in the disposition of atoms disappears [the distance r starting from a certain value $\rho(r) = \rho_0$]. The experimental areas of the coordination peak corresponding to the given distance r can be compared with the theoretical values calculated from the formulae

$$\Pi_T=2n_AZ_{AB}K_AK_B;\ \Pi_T=n_AZ_{AA}K_A^2, \quad (3)$$

where n_A is the number of atoms of kind A, which depends on the chemical composition, and Z_{AB} the coordination number, i.e. the number of atoms of kind B in the spherical shell bounded by the distances r and $r + d$ from the centre of the atom of kind A.

When the reliability criteria concerning the normalisation of the intensity curves hold and there is only a slight deviation from the series of approximations involved in the derivation of the principal formulae (the isotropic nature of the accumulation of atoms, the homogeneity of the medium, and infinite extent of the volume ensuring a statistically equiprobable environment of the atoms), the positions of the coordination peaks on the RDA curves are determined to within $\Delta r/r = \pm 0.5\%$ and the accuracy of the determination of the areas is to within ±5%.

Analysis of the RDA curves makes it possible not only to obtain the standard information described above but also to estimate the size of the crystallites when the latter is less than 30 Å. The determination is based on the fact that the form of the interference function for a high dispersity of the crystallites depends on their size. The form of the peaks on the scattering intensity curve and their resolution vary as a function of size.[32,33] For example, if the size of the metal crystallite with a face-centred cubic (FCC) lattice is 30 Å, then only 24 out of the 35 diffraction peaks are resolved. A change in the scattering intensity curve leads to a change in the RDA function. The coordination numbers in spherical particles of a metal with a face-centred cubic structure, whose diameters were multiples by factors of 3, 5, 7, etc. of the diameters of the individual atoms, have been evaluated by a statistical calculation.[34] With decrease in the size of the particles, there is a steady decrease in the area of the coordination peaks. For a particular size, there are consistent ratios of the areas. This feature has been used to estimate the sizes of highly disperse particles.[35–41] For a platinum particle diameter of 8 Å, the area of the first coordination sphere is half the value calculated for an infinite crystal, while the area of the second sphere is smaller by 30%; for a diameter of 30 Å, these areas are smaller by 15 and 25% respectively.

A characteristic feature of the calculation of the RDA curves by Moroz[20] is double normalisation (with respect to the far region of angles and with respect to the areas under the scattering intensity curves) and the use of experimental scattering factors. Criteria were developed for the reliability of the RDA curves as regards the normalisation of the X-ray scattering intensity and the intermediate parameters of the calculation.[20,42]

Experimental errors leading to failure of the reliability criteria were analysed, including the errors in the measurement of the intensity over a wide range of angles and at a single point (incorrect allowance for the contribution of the background and Compton scattering, the presence of fluorescent emission) and also the errors in the specification of the chemical composition.[20]

At the same time, procedures were developed for taking into account the contribution of the carrier to the overall X-ray scattering intensity curve and the RDA curve for the catalyst. Comparison of the curves for the intensity of the scattering of X-rays by the catalyst and the carrier is difficult owing to the different depths of the "working layer", because the catalyst contains as a rule a highly absorbing component. These disadvantages can be avoided if corrections are introduced in the analysis of the scattering intensity

curves for the background, polarisation, and absorption, and when the change to electronic units is made. The change to electronic units for the scattering intensity curve is an intermediate stage in the calculation of the RDA function and the construction of the difference intensity curve (DIC) then becomes possible.[20,42]

The determination of the dispersity of the active component in highly disperse deposited catalysts ($D < 30$ Å) is based on the analysis of the difference RDA curves. In principle, scattering intensity data are obtained by the RDA methods in the same way as in the usual precision measurements: the scattered X-ray intensity is measured over a wide range of angles with similar accuracies using monochromatic radiation. Short-wavelength molybdenum radiation with $\lambda K_{\alpha_1} = 0.71$ Å is usually employed. The intensity is measured for angles up to $2\theta = 160°$, which corresponds to $S_{max} = 4\pi \sin\theta_{max}/\lambda = 17.41$ Å.

The use of a monochromator leads to the loss of up to 80% of the intensity. The monochromator, ensuring a better relation between the signal and the background, does not transmit Compton (incoherent) scattering for angles $\theta > 20°$. For smaller angles, the monochromator transmits the entire Compton scattering, but in this region the Compton scattering itself is small.[27,43]

Conditions for an automated experiment with computer calculations have been described. The experiment lasts ~50 h and requires the stable operation of the apparatus (diffractometers of the DRON-3,4 or HZG-4C, B, A type are usually employed). The successful application of the RDA method requires that the following conditions be maintained:

1. The structure of the system components under consideration must be simple; the set of different interatomic distances must be small and the coordination numbers must be large.
2. Heavy atoms, whose percentage content is high, must be present in the system.
3. The components must have a perfect structure (absence of defects and vacancies). Analysis of the RDA curves does in fact make it possible to discover the presence of imperfections in the structure as a result of the comparison of the observed and calculated curves.
4. Accurate chemical analysis is essential.
5. A model of the postulated structure is needed.

The RDA method examined has been used successfully in the study of highy disperse systems of different chemical composition. However, the rigorous requirements which must be met by the experiment (monochromatisation, correct allowance for incoherent scattering, duration of the experiment) and by the preliminary treatment of data (careful normalisation of the scattering curves) and the ambiguity of the interpretation of the RDA curves limit the possibilities of this method in normal X-ray laboratories.

A high-speed method for the determination of atomic radial distribution functions, based on the *a priori* assumption that the functions of the background incoherent and independent gas scattering are monotonic, is being developed at present. This method does not require the measurement of the background and the knowledge of the intensity of the Compton scattering. The structure-sensitive part of the intensity curves is isolated with the aid of the cubic B-spline minimised by the method of least squares.[44] The method has been tested on polycrystalline silver and palladium.[45] The Fourier analysis of the structure-sensitive part of the intensity curve is used to obtain radial distribution functions by a procedure similar to that used in the Fourier transformation of the function of the long-range fine structure of the X-ray absorption spectrum in the EXAFS method, used to obtain structural information.[46,47] The proposed method makes it possible to accelerate and simplify the procedure involving the collection and treatment of experimental data (the experiment can be carried out without a monochromator, with a β-filter, and the normalisation of the intensity curves is also not needed). However, it cannot be used to establish the structural parameters of unknown materials, because it does not permit the determination of the absolute values of the coordination numbers. This method can be employed to analyse the changes in the structural characteristics in a series of specimens.

2. The method based on the full-profile X-ray analysis

About 20 years ago, a new effective method for the interpretation of powder diffraction data, called the Rietveld method,[48] appeared in neutron diffraction. It was subsequently used also in X-ray diffraction.[49–52]

The FPA method is based on the minimisation of the difference between the experimental and calculated diffraction patterns at any point on the X-ray diffraction pattern profile.

The function

$$\Phi = \sum_i^N W_i (y^e - y^t)^2,$$

is minimised by the methods of least squares. Here y^e and y^t are respectively the experimental and calculated intensities at the ith point of the profile, w_i is the weighting function, and N the number of points on the profile. Next, a sequence of corrections to the parameters of the specified model, converging to zero, is calculated. The summation in terms of the matrix elements of the least squares method is carried out over all the points on the profile included in the calculation. A series of matrices with the specified weighting factor are added to the matrix thus constructed. These matrices take into account the limitations to the ranges of variation of the interatomic distances and the equality of the bond lengths between various atoms, atoms in special positions being included in the calculation.[53] Since a non-linear relation between the parameters is fitted by a linear relation in the least squares method, it is essential to carry out several refining cycles.

The unreliability factors are used to estimate the reliability of the model:

$$R_p = \sum_i^N |Y_i^e - kY_i^t| \Big/ \sum Y_i^e \quad \text{(profile-based factor)}$$

and

$$R_I = \sum_i^N |I_i^e - kI_i^t| \Big/ \sum I_i^e \quad \text{(intensity-based factor)}$$

The factor R_P is found by summation over all the points of the profile and R_I by summation over the intensities of the diffraction lines. R_P usually exceeds R_I by a factor of two, while R_I is in its turn greater than the unreliability factor R_F, used in the single crystal method, by a factor of 1.5–2.

We used a computer program written in FORTRAN for the BESM-6 computer,[53,54] which includes the program published by Clark, et al.[55]

The entire X-ray diffraction pattern can be represented as a linear combination of the profiles of individual peaks. The overall intensity at each point on the pattern is described by the expression

$$Y_i^t = k \sum_j^N Y_j \Omega_{ij} + Y_i^\Phi,$$

where Ω_{ij} is the peak shape function, k the reduction coefficient, Y_i^b the background at the ith point, and Y_j the intensity of the jth reflection.

A line diagram based on the specified model is used for the construction of the theoretical profile (this requires the knowledge of the unit cell parameter, the symmetry space group, and the atomic coordinates).

The theoretical intensity is calculated by the formula

$$I_{hkl}=F_{hkl}^2 LPGn,$$

where L, P, and G are the Lorentz, polarisation, and geometrical factors respectively, n is the repeatability factor, and F_{hkl}^2 the structure factor. The structure factor is calculated in a general form in accordance with the formula

$$F_{hkl}^2=\left[\sum_{j=1}^{N} f_j\mu_j T_j \exp 2\pi i(hx_j+ky_j+lz_j)\right]^2$$

where x_j, y_j, and z_j are atomic coordinates, f_j is the atomic factor, μ_i the multiplicity of the atoms, T_j the thermal multiplier, and h, k, and l are the reflection indices.

Next, the line diagram is smeared by the function of the profile, which has parameters depending on the reflection angle. The neighbouring reflections contribute to the intensity at each point on the diffraction pattern. The main difficulty in the application of the Rietveld method involves the description of an individual profile of a reflection, since, in contrast to neutron diffraction, where Pearson's *YII* functions are used successfully, a similar unique theoretically well-founded function has not yet been proposed in X-ray diffraction. This is associated with the fact that the diffraction peaks corresponding to different reflection angles have different shapes and the experimental dependence of the peak half-width on the angle θ is not monotonic owing to effects caused by the real structure of the polycrystalline material (microdistortion, smallness of the coherent scattering regions, anisotropy, packing defects).[50,56–58] The majority of investigators[56,59–61] assume that a single profile is described most successfully by the generalised Pearson function:

$$P_{ij}=2\left(\frac{2^{1/m}-1}{\pi}\right)^{1/2}\frac{\Gamma(m)}{\Gamma(m-1/2)}H_j^{-1}\left[1+4\frac{(2\theta_i-2\theta_j)^2}{H_j^2}(2^{1/m}-1)\right]^{-m},$$

where Γ represents gamma-functions, H_j is the peak half-width (the width of the peak at the level of half its height); the power exponent m may be refined.

In our calculations, we used the version with $m = 2$ whereupon the Pearson function becomes a modified Lorentz function:

$$ML(2\theta_i, 2\theta_j)=\frac{2^{1/2}-1}{\pi H_j}\left[1+\frac{4(2^{1/2}-1)}{H_j^2}(2\theta_i-2\theta_j)^2\right]^{-2}.$$

According to Vainshtein's formula,[14] the dependence of H_j on θ_j has the form

$$H_j^2 = u\tan^2\theta + v\tan\theta + w.$$

The parameters u, v, and w are found from individual reflections and are refined.

In the FPA method, there are also other approaches, in particular the synthesis of the diffraction profile on the basis of specified instrumental, spectroscopic, and physical experimental parameters.[62] All the calculations are carried out in terms of Fourier coefficients, which ensures sufficient accuracy and speed. This approach made it possible to determine not only the structure but also the substructure parameters of substances.[63]

The FPA method is useful in the solution of many problems involving the refinement of structures whose type is already known. Such problems include the distribution of isomorphous impurities, the ordering of defects, the distribution of cations in spinels and other compounds, etc.[64–70] However, examples of the application of this method in the determination of unknown structures of new compounds also exist.[71–73]

The following structural parameters can be determined by the FPA method: (1) the atomic coordinates in fractions of the cells x, y, and z; (2) the overall thermal parameter (Q); (3) individual isotropic thermal factors of the ith atom; (4) the coefficient of the occupation of a given site by the ith atom (n_i); (5) the scaling coefficient (k).

In addition, a series of profile parameters, determining certain characteristics of the specimen and of the recording, can be refined: (1) the line half-width parameters u, v, and w; (2) the overall shift of the X-ray diffraction pattern relative to the origin z; (3) the lattice parameters A, B, C, α, β, and γ; (4) the asymmetry parameter P; (5) the texture parameter G; (6) the ratio of the intensities of the radiation components K_{α_1} and K_{α_2} (after passage through the monochromator, $I_{K_{\alpha_1}}$ and $I_{K_{\alpha_2}}$ may not be 2).

The experimental data obtained by the FPA method as well as the RDA method consist of measurements for individual points. The scanning step is determined by the line width (usually 0.01–0.05°). The use of Soller slits is obligatory. For a reliable determination of the profile parameters, it is recommended that individual peaks and non-doublet K_β radiation be employed.[67]

3. The method involving the determination of substructural characteristics

The method involving the determination of substructural characteristics (sizes of crystallites and their microdistortions, parameters determining the size distribution of crystallites), based on the harmonic analysis of the diffraction peak profiles, can be applied to systems of virtually any chemical composition in which the size of the crystallites is 30–1000 Å. An important feature is the fact that the substructural characteristics listed above refer directly to the component investigated (metal, oxide, salt, etc.) in the system under consideration.

The role of all the experimental factors influencing the profile of the diffraction maximum, such as the width of the slits on the collimator in the tube and in the counter, the focussing conditions etc. has been examined in detail.[74,75]

For a clear-cut differentiation of the profiles of the diffraction lines for the phase investigated, it is essential to carry out precision measurements of the line intensity at each point, which is achieved by scanning over the points with accumulation of a large number of counts. The lines are focussed using the 1:2:0.25 slit on the goniometer and monochromatised non-doublet CuK_β radiation (the monochromator is a flat graphite plate) in the range of angles exceeding by a factor of ~5 the half-width of the diffraction maximum. This is necessary in order to avoid additional errors associated with the numerical analysis of a profile of complex shape. The wide range of scanning angles ensures a satisfactory

determination of the line "tails", which is essential for the accurate determination of the Fourier coefficients. The correct determination of the profile of the instrumental line is very important.[76] Corondum (α-Al_2O_3) or silver black are chosen as reference standards. Their line profiles are described by the function

$$b^2 = u\tan^2\theta + v\tan\theta + w,$$

where u, v, and w are constants and θ is the Wulff–Bragg angle.

The substructural characteristics of deposited catalysts must be determined in four stages. The first stage consists in the separation of the diffraction maxima of the active component from the background due to the presence of the carrier. In the course of such treatment, the catalyst and carrier intensity curves are normalised and the background due to the carrier can be fitted by a polynomial. In the case of a single-phase system (for example, a metallic black) the problem simplifies and involves the usual separation of the background from the diffraction maximum.

The second stage reduces to the isolation from the experimental curve of the intensity of the profile associated with the physical broadening of the line (allowance for the instrumental line width). The third stage involves the finding of the fraction of the physical broadening of the line associated solely with the fine dispersity of the system (allowance from microdistortions). Warren's method is used for this purpose.[77] The method involving the expansion in Fourier series of the functions describing the profiles of the diffraction maxima of the reference standard and the test specimen is used in the second and third stages.

The parameters of the size distribution of the crystallites or the distribution function are found in the fourth stage. The profile of the diffraction maximum depends in principle on the crystallite size distribution function. However, according to Guinier,[78] the distribution of the lengths of sections in the crystallite (chords) perpendicular to the reflecting plane can be determined directly from the X-ray line profiles. It has been suggested[79] that the *hkl* line profile, determined by the reflection from crystallites, coincides with the profile of the diffraction line which arises in the presence of a set of parallel and incoherent linear sections. The ratios of the lengths of these sections must be the same as those of the chords of the grains perpendicular to the reflecting [h, k, l] plane. According to Bertaut's formula,[79] the intensity of the diffraction maximum is

$$I(x) = \int_0^\infty \frac{\sin^2 \pi A m x}{(\pi A x)^2} q(m)\, dm,$$

where $x = \theta - \theta_y$ is the angular scattering relative to the centre of gravity of the lines for the angle θ, $q(m)$ the function of the probability of the distribution of the lengths m of the chords perpendicular to the reflecting plane of the lattice in the set of crystallites, $A = (2\cos\theta)/\lambda$, θ is the Wulff–Bragg angle, and λ the radiation wavelength. The use of this equation presupposes that only the part of the physical broadening caused by the small size of the crystallites enters into the diffraction maximum profile. The profile is deduced from Fourier coefficients and normalised:

$$f_N(x) = f(x) \Big/ \int_{-\infty}^{\infty} f(x)dx.$$

The normalised function has a number of properties.[80] Thus, for $x = 0$ (at the maximum), we have $f_N(0) = 1/\beta = DA$, where $D = \lambda/2\beta\cos\theta$ is the average effective size of the crystallites (according to the Selyakov–Scherrer procedure) and β is the integral half-width of the line profile. The normalised function $f_N(x)$ is related to the function $I(x)$ by the expression

$$I(x) = (M_1/A) f_N(x),$$

where M_1 is the first moment of the chord length distribution function $q(m)$. The moment of any order of the chord length distribution function

$$M_n = \int_0^\infty m^n q(m)\, dm, \qquad M_2 = I(0)$$

can be expressed in terms of M_1:

$$M_{n+2} = (n+1)(n+2) M_1 \int_0^\infty m^n h(m)\, dm,$$

where $h(m)$ is the cosine component of the Fourier transformant $f_N(x)$.

Thus, knowing the diffraction maximum profile, it is possible, in principle, to determine the parameters characterising the size distribution of the crystallites, because the moments of the chord distribution curve can be determined on the basis of these data. The function itself can be deduced from the moments of the distribution curve. The quantity $V = M_2 - M_1^2$ characterises the variance of the distribution. In a study[8] using various methods of describing the distribution, such as the δ-function, the Gaussian function, the overall logarithmic distribution, and the lognormal distribution, it has been shown that the last distribution describes correctly the distribution of the chords in metallic particles on different carriers. The quality of the fit is characterised by the reliability coefficient. In our investigation,[81] it was also suggested that the chords present in the set of crystallites obey the lognormal distribution law (LND):

$$q(m) = \frac{1}{\sigma\sqrt{2}\,\pi m} \exp - \left(\frac{\ln m - \ln \mu}{2\sigma^2} \right).$$

The parameters μ and σ of the distribution can be obtained from the moments of the distribution curve $q(m)$ by means of the formula

$$\mu = M_1^2/\sqrt{M_2}, \quad e^{\sigma^2} = M_2/M_1^2.$$

A computer program was devised to interpret the experimental data. The following input information is used: (1) the intensities of two X-ray lines, of the specimen and the reference standard, the initial and final scanning angles, the scanning steps for the specimen in the reference standard, and the number of Fourier coefficients which must be calculated; (2) the range of the expansions; (3) the positions of the line maxima (either the position itself is specified or the centre of gravity is calculated); (4) the lattice parameter and Young's modulus. Young's modulus is required for the calculation of the microdistortions using the two lines corresponding to reflections from the [h, k, l] plane in different directions.

The calculated output data are as follows: (1) the Fourier coefficients of the initial lines of the specimen and the standard, the Fourier coefficients of the true physical broadening of each line, and the Fourier coefficients of the broadening due to the block structure

and microdistortions; (2) the curves deduced for the true physical broadening and the block structure normalised with respect to area; (3) the moments of the chord size distribution curve; (4) the distribution of the microdistortions; (5) the average particle size calculated from the Selyakov–Scherrer formula using the integral half-width of the function of the broadening induced by the block structure; (6) the positions of the centres of gravity of the initial lines.

Knowing the LND parameters μ and σ, it is possible to find (1) the most probable size of the crystallites m_0, (2) the average size of the crystallites in the bulk phase m, and (3) the area of the surface formed by the set of crystallites.

Thus the method involving the determination of substructural characteristics, based on the harmonic analysis of the diffraction peak profiles, yields information about the sizes of the crystallites, which exceed by a factor of 10^3 the wavelength, the microdistortions of the crystallites equilibrated in the bulk phase, and the parameters determining the size distribution of the crystallites. An important case of the breakdown of order in the crystal is that of the planar disorder. This is particularly important for close-packed structures or structures made up of planar networks superimposed in accordance with a definite law. The deviations from the general law governing the deposition of layers relative to one another in such structures influence significantly the diffraction line profiles.[76,78]

In principle all the characteristics obtained by the method considered, apart from the size of the microdistortions, can be determined with the aid of an electron microscope. However, the electron microscope method is local in scope and requires the availability of a large statistical set of data. Furthermore, the electron beam can affect small particles with a low melting point. The surface area of metals on carriers can also be determined by the chemisorption method. However, it is subject to a series of limitations determined by the assumptions underlying it. The application of this method presupposes the selective nature of the adsorption, the knowledge of the stoichiometric coefficient for the chemisorption of the adsorbate, and the availability of information about the number of surface metal atoms. The method involving the determination of substructural characteristics is usually employed to establish the size of the crystallites and of the microdistortions equilibrated within the bulk of the crystallite. We were able to supplement this information by data concerning the size distribution of crystallites.[81–83]

III. Structural and substructural characteristics of catalyst carriers

1. Aluminium oxides

(a) Low-temperature forms

The dehydration of the initial aluminium hydroxides above 473 K gives rise to the formation of different low-temperature forms of the oxides, depending on the nature of the hydroxides: amorphous, χ, γ, ρ, and η. In terms of their structure, these oxides are defective spinels, in the structure of which 21.33 cations are distributed among 24 cationic sites. In conformity with the requirements of stoichiometry and electroneutrality, they are described by the general formula $Al_{8/3}\square_{1/3}O_4$. The differences between the forms are manifested by the distribution of vacancies among the cationic sites. It has been suggested that the vacancies in γ-Al_2O_3 are located preferentially in octahedra, while those in the η-forms are in tetrahedra.[84–89]

The diffraction patterns of the low-temperature forms of aluminium oxide, obtained from pseudoboehmite, bayerite, and gibbsite, differ only slightly from one another. Characteristic regions exhibiting differences in the diffraction pattern correspond to each form. Analysis of these differences constitutes the basis of quantitative phase analysis.[20,90,91]

The RDA curves for the low-temperature forms differ from one another less than the corresponding scattering intensity curves (the RDA curve for the amorphous phase obtained from the deposited hydroxide is an exception).[20,92–94] This indicates the similarity of their structures and the equality of the interatomic distances and of the coordination numbers in the first coordination spheres.

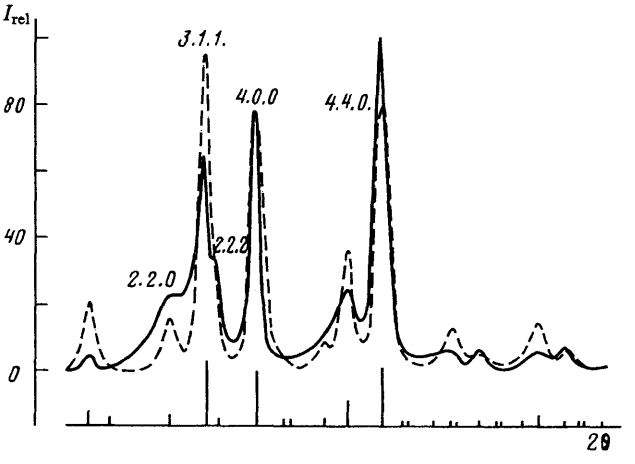


Figure 1. Fragments of the experimental (continuous line) diffraction pattern of η-Al_2O_3 and the pattern calculated on the basis of the defective spinel model with vacancies (dashed curve).[96]

We investigated by the FPA method the structures of the low-temperature oxides obtained from boehmite, pseudoboehmite, and bayerite.[95,96]

Models of defective spinels with different distributions of vacancies were used as the initial models for the calculation of the diffraction patterns: in octahedra—$Al[Al_{13.33}\square_{2.67}]O_{32}$ and in tetrahedra—$Al_{5.33}\square_{2.67}[Al_{16}]O_{32}$. The calculations were carried out within the framework of the space group $Fd3m$ with the origin of coordinates at a tetrahedral cation. Fig. 1 presents the experimental diffraction pattern of η-Al_2O_3 and the pattern calculated on the basis of the spinel with vacancies model. Evidently the most intense experimental line is 4.4.0, whereas according to the calculation the most intense line should be 3.1.1. Furthermore, the experimental intensity of the 2.2.2 line is appreciably higher than the calculated intensity. The difference between the calculated and experimental densities is also significant: the calculated density is 3.62 g cm^{-3}, while the experimental densities range from 3.35 to 3.42 g cm^{-3} for different forms. The unreliability factor R is about 40% for both models described by the general formula $Al_{21.23}\square_{2.67}O_{32}$. A change in the distributon of vacancies between the tetrahedral and octahedral sites does not reduce R.

In the real structures of the low-temperature oxides, an appreciable proportion of the anions exist as OH^- groups. Having included these groups in the structure, it is possible to describe the oxides by the general formula $Al_2O_3.nH_2O$, where $0 < n < 0.6$. According to this formula, the ratio of the numbers of cations and oxygen atoms is altered and this makes it possible to consider formally another spinel structure with a greater number of cationic vacancies. By varying the number of these vacancies in the range from 2.67 to 6.5, which corresponds to a number of water molecules between 0 and 0.6, it is possible to reduce the R factor to ~30% for the optimum number of vacancies of about 5. Variation of the distribution of vacancies among the cationic sites within the limits indicated does not reduce the R factor.

The space group $Fd3m$ permits the existence of two pairs of cationic sites when the origin of coordinates is selected at the point $\bar{4}3m$: it is possible to select the coordinates A(0; 0; 0) or A*(0.5; 0.5; 0.5) for the eightfold site (tetrahedra) and B(0.625; 0.625; 0.625) or B*(0.125; 0.125; 0.125) for the sixteenfold site (octahedra). The use of only the coordinates A* and B* is equivalent to a shift of the origin of coordinates, which naturally does not alter the R factor. A model of the type $A^*_{x_1}A_{x_2}B^*_{y_1}B_{y_2}O_{32-z}(OH,...)_z$ was examined. It follows from steric considerations that the use of type A* coordinates is possible only when the four nearest octahedral cations B are removed simultaneously. The disposition of the cations B* requires in its turn the removal of two nearest cations A displaced relative to one another by a vector with the coordinates 0.25; 0.25; 0.25. The B* atom is then located at the centre of the vector.

Several models of the structures of the low-temperature oxides were calculated. The data for modelling the η-Al_2O_3 structure are presented in Table 1, which also indicates the unreliability factors and the calculated densities. It follows from the Table that the lowest unreliability factor corresponds to the structural formula

$$A^*_{1.5}A_{6.75}B^*_{1.0}B_{10.0}O_{32-z}(OH,\ldots)_z,$$

where A and B are the spinel cationic sites and A* and B* are the non-spinel cationic sites.

Table 1. Modelling of the η-Al_2O_3 structure.

Parameter	1	2	3	4
x_1	–	–	–	1.5
x_2	5.66	8.0	7.75	6.75
y_1	–	–	–	1.0
y_2	16.0	13.66	11.5	10.0
R	45.6	44.7	34.1	10.1
d, g cm^{-3}	3.60–3.70		3.33–3.35	

Note. The following notation has been adopted for the models: 1, $A_{5.66}\square_{2.33}B_{16}O_{32}$; 2, $A_8B_{13.66}\square_{2.33}O_{32}$; 3 and 4, $A^*_{x_1}A_{x_2}B^*_{y_1}B_{y_2}.O_{32-z}(OH,...)_z$.

Table 2 presents the structural formulae and data for the distribution of cations in the low-temperature oxides. It is striking that anionic modification of the low-temperature oxide (inclusion of OH groups in the anionic skeleton) entails cationic modification (new positions of the aluminium cations). Such compounds are referred to as "protospinel" compounds.[97]

Table 2 shows that the fraction of tetrahedral cations is almost the same in all the forms (0.4–0.46). The greatest number of filled tetrahedra (8.5) combined with the smallest number of filled octahedra (10.0) occurs in the $\gamma_{\pi/\sigma e}$-Al_2O_3 form. In terms of the ratio of the numbers of tetrahedra and octahedra the oxides can be arranged in the series $\gamma_{\pi/\sigma e} > \eta > \gamma_{\sigma e}$.

Table 2. Structural formulae and the distribution of cations in low-temperature aluminium oxides.

Form of oxide	Fraction of tetrahedra (T)	Fraction of octrahedra (O)	T/O	A+B	A*+B*	$\frac{A+B}{A^*+B^*}$
$\gamma_{\sigma e}$	0.40	0.60	0.66	14.5	3.75	3.9
$\gamma_{\pi/\sigma e}$	0.46	0.54	0.85	15.75	2.75	5.7
η	0.43	0.57	0.75	16.75	2.5	6.7

Note. The following forms of the oxides were examined:

$\gamma_{\sigma e} - A^*_{1.75}A_{5.50}B^*_{2.0}B_{9.0}O_{22.75}(OH,\ldots)_{9.25}$;

$\gamma_{\pi/\sigma e} - A^*_{1.75}A_{6.75}B^*_{1.0}B_{9.0}O_{23.5}(OH,\ldots)_{8.50}$;

$\eta - A^*_{1.50}A_{6.75}B^*_{1.0}B_{10.0}O_{23.75}(OH,\ldots)_{6.25}$.

Thus on the basis of the real diffraction pattern and using the method of the full-profile analysis, we established that the low-temperature forms γ- and η-Al_2O_3 cannot be described as spinel-type structures with a statistical or regular distribution of vacancies. If the space group $Fd3m$ is adopted as a basis, then the above forms can be regarded as structures in which two allowed tetrahedral and two allowed octahedral sites are filled statistically. Each form has its own characteristic number of anions consisting of hydroxy-groups or other residual groups of the type NO_3^-, Cl^-, etc.

The OH groups were regarded[98] as the structural elements of the low-temperature forms, but it was assumed that there are vacancies in the cationic sublattice: $Al_{20}\square_4O_{28}(OH)_4$. Using the general Debye formula for the scattering intensity and comparing the synthesised and experimental diffraction patterns, Espinat, et al.[99] confirmed the validity of the model of γ-Al_2O_3 described above.

(b) High-temperature forms

The high-temperature δ- and θ-forms of aluminium oxide are also used widely as carriers for catalysts of high-temperature processes. They are produced from γ- and η-Al_2O_3 by dehydration at temperatures above 1100 K. It has been shown by the RDA method[94] that, together with the loss of OH groups, dehydration involves a rearrangement of the structures associated with a decrease and increase in the filling of the octahedral and tetrahedral cationic sites respectively. Under these conditons, new cationic sites, uncharacteristic of the low-temperature forms, are filled. The high-temperature aluminium oxides differ in the filling of the cationic sites and are described by the general formula $E_RA^*_{x_3}A_{x_4}B^*_{y_3}B_{y_4}O_{32-f}(OH,...)_f$, where $R + x_3 + x_4 + y_3 + y_4 < 21.33$ and f is the number of structural OH and other groups. The

formation of the δ- and θ-forms can be regarded as a result of the structural compensation for the partial removal of hydroxy-groups and other anionic "impurities" during the complete dehydration of the hydroxides to anhydrous α-Al_2O_3.

(c) Promoted aluminium oxides

The refinement of the structures of the low-temperature aluminium oxides made it possible to put forward a hypothesis concerning the mechanism of the formation of the solid solutions and non-stoichiometric spinels obtained when cations and anions are introduced. Since all the ionic sites in the structures of the oxides are characterised as regards their positions in the cell and the degree of their filling, it is possible to construct models of the hydroxide oxide compounds modified by cations and anions.

The polymorphic transformations occurring on aluminium oxides have been investigated[100–106] and the phase compositions and structures of the low-temperature oxides promoted by divalent and trivalent cations (Mg^{2+}, Ni^{2+}, Cu^{2+}, Cr^{3+}) have been analysed. It has been shown[102–104] that the low-temperature solid solutions are formed in these systems as a result of the filling of the vacancies in the bulk-phase structure of the spinel and by the substitution of certain tetrahedral and octahedral sites in the structure of the protospinel. The substitution of aluminium by a divalent cation in the protospinel structure, without a distinct preference for an octahedral or a tetrahedral environment, leads to the breakdown of the electroneutrality of the Al_2O_3 molecule. The excess charge can then be compensated either by an increase in the number of hydroxy-groups in the anionic skeleton (on formation of mixtures of hydroxides by coprecipitation) or by the removal of some of the anions, i.e. OH^- and NO_3^- (during heat treatment). In both cases, a general disordering of the structure, in particular of the anionic skeleton, is observed, which is manifested by a frequently noted broadening of the diffraction maxima. Another way of compensating for the excess charge is also possible. This can be achieved if the cations occupy preferentially the tetrahedral sites and involves a rearrangement of the cationic skeleton. Such rearrangement can be attained by the migration of aluminium from the A* and B* sites to the A and B sites respectively and the disposition of the divalent cations in the A sites. This results in the formation of a normal spinel of the type AB_2O_4. The location of the divalent cation in a tetrahedral site A does not require structural compensation, because it corresponds to the arrangement typical for a spinel. In such systems an increase in temperature does not entail the formation of the intermediate δ- and θ-forms of Al_2O_3.

The distribution of cations in the structure of an alumino-magnesium spinel with a non-stoichiometric composition was refined[107] by the FPA method. The magnesium and aluminium cations were detected at sites uncharacteristic of a spinel. These cations are regarded as point defects. It was established by the method involving the determination of substructural characteristics that the dominant type of defects in the specimen is packing defects caused by half-dislocations, whose concentration is virtually identical with the concentration of the detected point defects. The presence in the specimen of specific extended defects, whose orientation is identical with that of the half-dislocation vector, was confirmed by high-resolution electron microscopy. The non-stoichiometric aluminomagnesium spinel was investigated by a version of the FPA program, in which provision is made for the possibility of refining individual profile parameters of the diffraction peaks. The solution of this problem can also be assisted by the application of the versions used in other studies.[68,108]

2. Carbon carriers for catalysts

Carbon materials are widely used as sorbents, but recently porous carbon materials have come to be used also as carriers for metallic catalysts and as catalysts themselves. The study of the structural and substructural characteristics of these materials is extremely important for the elucidation of their adsorption and texture characteristics in order to achieve an understanding of the chemistry of their surfaces. The carbon materials investigated include Sibunit, Altunit, activated charcoals (from Saran plastic and birchwood), acetylenic carbon black, and brown coal semicoke.[20,109–111]

The following characteristics were determined for Sibunit: degree of crystallinity K = 0.65, fraction of aromatic carbon A = 1.0, degree of three-dimensional order γ = 0.3, size of crystallites in the plane of aromatic layers L_a = 35 Å, size of crystallites in the direction at right angles to the plane of aromatic layers (thickness of packets of layers) L_c = 40 Å. The size distribution of the particles was determined for Altunit by X-ray diffraction, which yielded a variance of the distribution V = 230 Å^2, the average particle size L = 20 Å, and the most probable particle size m_0 = 10 Å. It was established that microdiffraction does not occur in Altunit. It was suggested that Silbunit has a graphite-like structure, while Altunit has a diamond-like structure. The interatomic distances r and coordination numbers were calculated for these structures and were determined from the RDA curve (Tables 3 and 4).

Table 3. Structural characteristics of Sibunit.[20]

r, Å		C.N.	
expt.	calc.	expt.	calc.
1.44	1.42	2.2	3
2.44	2.46	6.0	6
2.90	2.84	3.6	3
3.36	3.37	2.5	2
–	3.66	—	12
3.78	3.76	13.1	6
–	4.17	diffuse	12
4.29	4.26	peaks	6
–	4.41	ditto	12
4.88	4.92	"	6

Table 4. Structural characteristics of Altunit.[20]

r, Å		C.N.	
expt.	calc.	expt.	calc.
1.58	1.54	2.4	4
2.54	2.52	11.4	12
3.02	2.96	10.1	12
3.46	3.57	3.0	6
3.90	3.89	10.0	12
4.38	4.37	22.0	24
4.78	4.63	16.0	16
5.22	5.28	24.0	24
5.74	5.64	24.3	24

Examination of Tables 3 and 4 showed that Tibunit has a somewhat disordered graphite structure while Altunit has the diamond structure. A globule 35 Å in diameter is a coherently scattering element in Sibunit, which corresponds to ~100 unit cells. The layered structure is retained in such a globule, but the interlayer distance along the c axis has increased owing to the azimuthal disorientation of the graphite networks. Together with the three-dimensionally ordered crystalline carbon, the specimen contains also carbon in the form of two-dimensional hexagonal formations, i.e. the entire carbon is aromatic (A = 1).

The diamond structure of Altunit is characterised by an increased unit cell parameter a (Δa = 0.007 Å). This change is apparently associated with the high dispersity of the material (the size of the crystallites is ~20 Å). An important characteristic of Altunit is the absence of microdistortions equilibrated in the bulk of the crystallite. The [size] distribution of the particles in this material is fairly narrow.

Carbon carriers also include activated charcoals differing in their porous structure: Saran and birchwood charcoals, brown coal semicoke, and acetylenic carbon black.[112] The Saran charcoal has the most perfect structure; the highest degree of three-dimensional order (γ = 0.3) and high degrees of aromaticity and crystallinity are characteristic of this material. The RDA curves for the above carbon materials show that the Saran charcoal is also distinguished by a more pronounced long-range order than, for example, acetylenic carbon black, which exhibits a weak three-dimensional order and a low aromaticity and crystallinity.

IV. Structural and substructural characteristics of deposited and non-deposited monometallic catalysts

The development of X-ray diffraction methods for the study of highly disperse systems and refinement of the structures of catalyst carriers have made it possible to carry out precision analyses of highly disperse metal–carrier systems. In the course of such investigations, it was essential to answer the question whether the metal–carrier system is additive and whether it is permissible to use the structural and substructural characteristics of highly disperse non-deposited metals (blacks) in the study of deposited particles. Can blacks serve as reference standards for the construction of difference RDA curves? What is the role of the carrier in the stabilisation of the active component?

Table 5. Substructural characteristics of metal blacks.[81,82]

Crystallographic direction	L, Å		$10^{-2} \cdot V$, Å^2		m_0, Å		$10^3 \cdot \varepsilon$	
	Pt	Pd	Pt	Pd	Pt	Pd	Pt	Pd
[111]	38	370	9.8	111	16	330	3.8	1.2
[100]	38	215	4.8	50	22	180	3.8	1.4

The study of the structural and substructural characteristics of highly disperse and non-deposited metals (Pt, Ir,[35,81] Pd,[82] and Ni[112]) showed that, as the size of the crystallites decreases from 700 to 40 Å, the coordination peaks (CP) on the RDA curves are broadened and their area diminishes. The mean square displacements of the atoms relative to the equilibrium position are ~3% of the shortest distance. Analysis of the RDA curves showed that the blacks exist in a polydisperse state, i.e. the coordination peak areas on these curves do not exhibit an unambiguous dependence on dispersity. The substructural characteristics of the non-deposited metals depend significantly on the average size L of the crystallites (Table 5): for large values of L, a wider size distribution of the crystallites is observed, mainly in the direction of the growth of the particles [111], while small particles are isotropic. Small crystallites are distinguished by greater microdistortions, which alter the structural characteristics—the unit cell parameter (by 3 × 10^{-3} Å) and the coordination numbers.[35]

The substructural characteristics of the non-deposited and deposited highly disperse metals were compared for aluminoplatinum catalysts and platinum blacks.[83] Model catalysts containing 3.8 wt.% Pt on γ-Al_2O_3 and blacks heat-treated at different temperatures were used as the objects of study. Table 6 shows that the black and the non-deposited aluminoplatinum catalyst, heat-treated at the same temperature (773 K), are characterised by significantly different average sizes of the crystallites and variances of the size distributions of the particles. The size distribution of the platinum particles in the non-deposited catalyst is narrower.

Table 6. Comparison of the substructural characteristics of highly disperse deposited and massive metals.[83]

Specimen, heat treatment temperature	Pt, wt.%	S_{sp}, $m^2 g^{-1}$	Substructural characteristics			Microdistortions, $10^3\varepsilon$
			L, Å	$V \cdot 10^{-2}$, Å^2	m_0, Å	
Pt/Al_2O_3, 773 K	3.8	88±8	46	3.7	35	–
Pt/Al_2O_3, 1103 K	3.8	1	160	96	100	–
Pt black, 773 K	–	6±2	150	154	70	1.4
Pt black, 333 K	–	–	38	9.8	20	3.8

The structural characteristics of the non-deposited metals were obtained by the RDA method. Table 7 indicates the interatomic distances and the coordination peak areas as well as the sizes of the crystallites (L) for aluminoplatinum catalysts containing 2.4 and 7 wt.% Pt on γ-Al_2O_3. Analysis of the Table shows that only a certain proportion of platinum is present in the face-centred cubic structure of the metal and varies within the range 0.5–0.7. The ratios of the coordination peak areas corresponding to different coordination spheres (26:58:62:102 and 112:245:234:465) for catalysts with platinum contents of 2.4 and 7 wt.% respectively are close to the theoretical ratios 1:2:2:4. This shows that the metal particles are ordered and well crystallised.

Thus it follows from the comparison of the substructural and structural characteristics of the non-deposited and deposited metals that the carrier influences significantly the state of the metallic highly

disperse particles: the structure of the deposited particles is closer to ideality (the changes in the interatomic distances and coordination numbers characteristic of the blacks are not observed and there are no microdistortions). It becomes clear why the affinity of the adsorption isotherms on the deposited catalysts holds only when the crystallised black is used as the reference standard:[113] the metal on the carrier surface apparently exists in a micro-single crystal state, i.e. the similarity of the adsorption properties is a consequence of the identity of the structural and substructural characteristics.

Table 7. Theoretical and experimental interatomic distances (r) and coordination numbers for deposited aluminoplatinum catalysts.

Coordination sphere	C.N.	2.4% Pt/γ-Al_2O_3				7% Pt/γ-Al_2O_3			
		r, Å		CP area, el.^{2}		r, Å		CP area, el.^{2}	
		calc.	theory	calc.	theory	calc.	theory	calc.	theory
I	12	2.78	2.78	54	26	2.78	2.80	170	112
II	24	4.80	4.80	108	58	4.80	4.78	340	245
IV	24	6.21	6.20	108	62	6.21	6.16	340	234
VI	48	7.34	7.40	216	102	7.34	7.34	680	465
P_e/P_c^*		0.51				0.69			
L, Å		30				40			

*P_e/P_c is the ratio of the experimental and calculated coordination peak areas.

Comparison of the structural and substructural characteristics of the deposited and non-deposited metals shows that highly disperse blacks cannot serve as reference standards for the construction of the difference RDA curves in the study of the phase composition of deposited catalysts.

Catalysts containing 1.5–30 wt.% of platinum, iridium, and palladium on γ-, χ-, η-, and θ-Al_2O_3 [36–38,40,114–117] and on carbon carriers[39] were also investigated, the dispersity of the active component was estimated, and data were obtained for the phase compositions of the catalysts at different stages of their preparation. The dispersity and composition of the active component depend on the conditions in the preparation of the catalyst: when they are prepared by the method involving the impregnation of carriers with a solution of the metal-containing component, the temperature and composition of the gas phase play a significant role. After impregnation with a chlorine-containing substance and drying in air, a complex between the carrier and the $(MCl)_6^{2-}$ anion is formed in the catalyst, some of the chloride ions in the complex being replaced by hydroxy-groups. Activation by oxidative treatment at 723 K leads to the decomposition of the complex and an interaction phase, incorporating the metal ion, arises between the carrier and the active component. This phase has a spinel-like structure.[36,115] Metal ions are not distributed statistically on the surface of the carrier but are incorported in its structure. The reduced catalysts contain not only the metallic phase but also the interaction phase.

Fig. 2*a* presents fragments of the diffraction scattering intensity curves on the η-Al_2O_3 carrier and the 10 wt.% Ir/η-Al_2O_3 catalyst as well as the difference intensity curve (DIC). On the latter, there is a diffraction maximum due to iridium (0.2.2) (2θ = 69°2′) and the maximum (4.4.0) of the protospinel phase, the unit cell parameter of which has increased by 0.01 Å compared with that of the carrier. The position of the 0.2.2 line coincides with the theoretical position calculated for the iridium single crystal with a face-centred cubic latice. The RDA curve was plotted on the basis of the difference intensity curve (Fig. 2*b*). Together with the peaks corresponding to the interatomic distances in the face-centred cubic lattice of iridium (r = 2.7, 3.84, 4.70, 5.43, 6.07, 7.18 Å), the RDA curve contains a peak due to the protospinel interaction phase (r = 3.3, 4.2, 5.2, etc. Å). The amount of iridium incorporated in the form of ions in the interaction phase is determined by the overall content of the deposited metal, the structure of the carrier, and the temperature and composition of the gaseous medium. For a large iridium content in the ionic form, the specimens exhibit an enhanced chemisorption capacity in relation to hydrogen, which is associated with the additional adsorption of hydrogen on the modified carrier.[37,38]

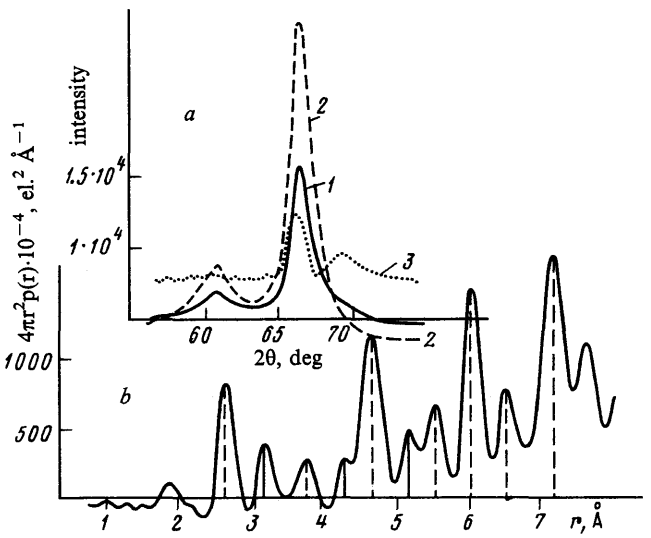


Figure 2. Fragments of the curves for the diffraction scattering of X-rays by the 10% Ir/η-Al_2O_3 catalyst (curve *1*) and the carrier (curve *2*) (in counts) and the difference intensity curve (curve *3*) (in electronic units) (*a*) as well as the difference RDA curve calculated from the difference intensity curve[42] (*b*).

The study of different deposited metallic catalysts showed[20] that in the general case the metal can exist in the following states: (a) as metallic particles distributed on the carrier surface; (b) as oxide particles or as an oxide film on the surfaces of large crystallites; (c) as the phase due to the interaction with the carrier, which is formed on activation (heat treatment with air) of the catalyst. The existence of these states and their thermal stability together with diffusional atom (particle) migration processes influence one of the most important characteristics of the deposited catalyst—the dispersity of the active component.

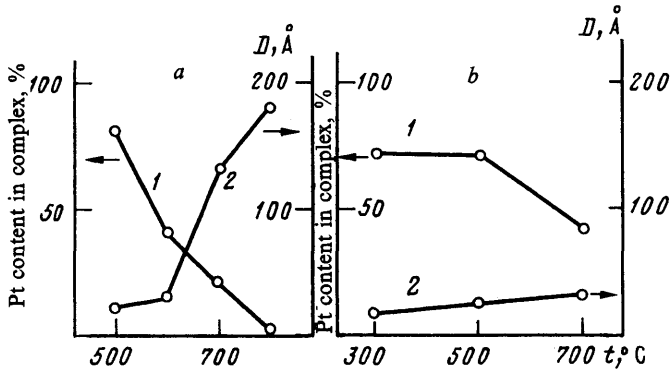


Figure 3. Dependence of the amount of Pt^+ (line *1*) and the Pt^0 particle size (line *2*) on the heat treatment temperature of the aluminoplatinum catalyst in oxidising (*a*) and reducing (*b*) gaseous media.[129]

Table 8. Certain characteristics of platinum catalysts on various carriers.

Carrier	Specific surface of carrier $m^2\ g^{-1}$	Pt^0/Pt^+	*L*, Å
γ-Al_2O_3	140	0.6	30
η-Al_2O_3	350	0.5	30
θ-Al_2O_3	70	0.4	30
SiO_2	300	1.0	100
C	600	0.4	30
$ZnAl_2O_4$	12	1.0	350

Fig. 3 presents the dependences of the sizes of the platinum crystallites *D* in the aluminoplatinum catalyst and of the amount of platinum incorporated in the interaction phase on the temperature in various gaseous media. In an oxidising medium (Fig. 3*a*), an antiparallel relation is observed between the amount of Pt^+ in the carrier structure and the dispersity of the metallic particles distributed on the surface. Evidently, the decomposition of the spinel-like phase results in the concentration of atoms on the surface and in the sintering of the active components. The decrease in the amount of platinum bound to the carrier apparently lowers the number of sites where the metallic particles are fixed on the carrier surface, which entails the sintering of these particles. A similar explanation was given, for example, in a study[118] of the role of ions as "energy traps" for metallic particles. In a reducing medium (Fig. 3*b*), a decrease in the amount of platinum bound to the carrier does not cause a sharp alteration of the sizes of the crystallites, because above 773 K an increase in the dispersity of the active component due to the dissolution of hydrogen in platinum is observed.[114] During phase transformations in the carrier, the interaction phase also decomposes, this being accompanied by the appearance of highly disperse metallic particles.[38] The Pt^0 and Pt^+ active centres exhibit definite catalytic activity: Pt^0 is active in the cyclohexane dehydrogenation reaction and Pt^+ is active in the dehydrocyclisation of n-heptane.[119,120] Table 8 presents the results of the comparison of the platinum impregnation catalysts deposited on sections of the carrier differing in their chemical nature and in their specific surfaces.

The Table shows that the amount of metal incorporated in the interaction phase is determined not by the surface area of the carrier but by its structure. The bulk-phase structure of the carrier determines also the number of reactive groups which can participate in the formation of the sites where highly disperse zerovalent metal particles are fixed.

V. Determination of the phase composition of deposited bimetallic catalysts

It is fairly difficult to obtain information about the structure of highly disperse bimetallic deposited catalysts, because mainly a comparative method is used for this purpose: the RDA curves for the carrier, the active component with the carrier, and the modifying element with the carrier are compared with the RDA curves for the bimetallic catalyst. The results of the X-ray diffraction study are therefore mainly qualitative and concern the phase composition. We shall consider the study of platinum–rhenium, platinum–tin, and nickel–tin catalysts.

1. Platinum–rhenium catalysts

Platinun–rhenium catalysts on γ-Al_2O_3, obtained by the impregnation method, were investigated by Ushakov, et al.,[121] who compared specimens containing only platinum, only rhenium, and a combination comprising 2 wt.% Pt + 0.8 wt.% Re. Analysis of the difference curves showed that (1) in both the bimetallic and aluminorhenium catalysts there is no metallic rhenium phase; (2) the areas of the coordination peaks for the platinum structure in the bimetallic catalyst are smaller than in the aluminoplatinum catalyst; (3) the areas of the coordination peaks for the carrier structure in the bimetallic system increase for the octahedral distances (Fig. 4). This permitted the conclusion that the rhenium in the bimetallic catalyst is present in the oxidised state (during preparation, the carrier interacts with rhenium ions) and the dispersity of platinum increases.

Analysis of the diffraction patterns recorded accurately by a procedure involving the accumulation of 2×10^5 counts did not reveal the shift of the diffraction maxima characteristic of the platinum–rhenium alloy. Platinum–rhenium catalysts on silica gel, obtained by the method involving the successive impregnation of the carrier with NH_4ReO_4 and H_2PtCl_6 solutions and the deposition of the organometallic complexes $[Re(OC_2H_5)_3]_3$ and $Pt(\pi\text{-}C_4H_7)_2$, were also investigated.[122]

Fig. 4 presents the RDA curves for the two specimens investigated. Im the impregnation specimen, the active component exists in a fairly coarsely disperse state: all the coordination peaks correspond, as regards their areas and positions, to the structures of the metallic rhenium and platinum, the Pt–Re alloy phase not being observed. The RDA curve for the catalyst obtained by the immobilisation of the platinum particles on the rhenium ion-modified silica gel surface has only the first coordination peak of the face-centred cubic structure of platinum. Hence it follows that platinum crystallises in a highly disperse state (the crystallite diameters are ~6 Å). The state of rhenium can be inferred from the coordination peak at r = 2.48 Å. This value of r corresponds to the

Re–Re distance in the trinuclear rhenium complexes used for the deposition of low-valence ions on the silica gel surface. The conclusions reached were confirmed by other physical methods (EXAFS, X-ray photoelectron spectroscopy, chemisorption).[123]

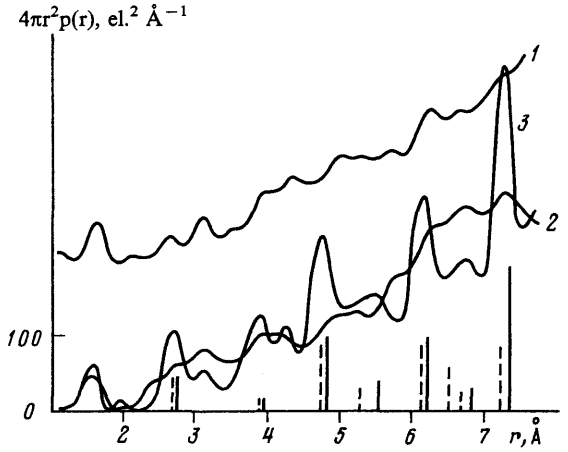


Figure 4. RDA curves for the SiO_2 carrier (curve *1*) and the platinum–rhenium catalysts obtained from organometallic compounds (curve *2*) and by the impregnation method (curve *3*).[123]

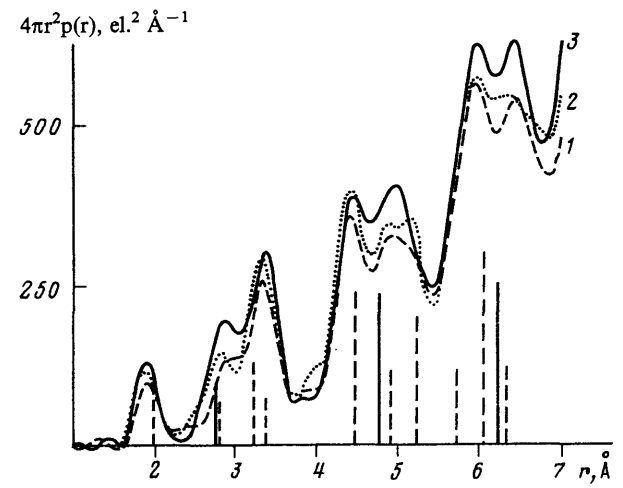


Figure 5. RDA curves for the γ-Al_2O_3 carrier (curve *1*), the aluminotin catalyst (curve *2*), and the aluminoplatinum–tin catalyst (curve *3*).[124]

2. Platinum–tin catalysts

In the course of the development of a thermostable and selective catalyst for the aromatisation of paraffinic hydrocarbons,[124,125] it was observed that the aromatising activity and stability of the catalysts synthesised by the interaction of platinum tetrachloride with low-valence tin ions stabilised on the aluminium oxide surface is appreciably higher than that of the reference catalyst prepared by the impregnation method. In order to elucidate the causes of the modifying effect of tin, a study was made of specimens containing 2.5 wt.% Sn and 2.6 wt.% Pt + 3.9 wt.% Sn on γ-Al_2O_3. The form of the RDA curves (Fig. 5) indicates the absence of the metallic tin phase and of Pt–Sn alloys.

The dispersity of the crystalline platinum phase is high (the size of the crystallite is ~10 Å) and tin is incorporated in the carrier surface, forming a spinel-like phase (the areas of the coordination peaks corresponding to the A–B, B–O, and B–B distances increase). Mössbauer spectroscopic data also confirmed that tin does not form an alloy with platinum but is present in the carrier structure. The effective charge on the platinum atoms decreases in the presence of Sn^{2+} ions (X-ray photoelectron spectroscopic data), which alters the adsorption and catalytic properties of platinum. The coordinatively unsaturated tin ions on the carrier surface are centres for the stabilisation of platinum atoms. The increase in the energy of the interaction of the active component with the carrier is indicated by the thermal stability of the active phase (the dispersity of platinum is close to the limiting value and persists for a long time up to a reduction temperature of ~873 K).

When silicon oxide modified by tin acetate is used as the carrier,[126] the phase composition of the active component is different: part of the tin ($\sim 1/3$) is reduced to the zerovalent state, forming the Pt_3Sn alloy, while the remainder is bound chemically to the SiO_2 surface. Thus the state of tin on silica gel is different than on γ-Al_2O_3. The catalytic properties are likewise different: the catalysts on γ-Al_2O_3 propagate the hydrogenolysis and aromatisation reactions at temperatures above 673 K and are inactive up to this temperature in benzene and cyclohexane hydrogenation reactions, whereas catalysts on SiO_2 are active in the former reaction already at 373 K and in the latter at 523 K.

The platinum–tin catalysts on a zinc–aluminium spinel are used for the single-stage dehydrogenation of lower paraffins to diolefins in water vapour at atmospheric pressure.[127] The study of the genesis of the phase composition of a catalyst containing 0.4–1 wt.% Pt + 1–5 wt.% Sn at all stages of their preparation showed that the gaseous medium used in the preliminary heat treatment affects significantly the composition of the catalyst. Reduction directly after drying of both monometallic and bimetallic catalysts (H_2, 848 K) leads to the formation of inactive intermetallic compounds with zinc (ZnO enters into the composition of the carrier as an excess phase), the composition of these compounds being determined by the ZnO content. After activation in an oxidising medium with water vapour, the X-ray diffraction patterns of the platinum–tin and monometallic platinum catalysts show the platinum lines corresponding to the normal unit cell parameter. Tin is then present in an oxidised state. With increase in the zinc content, there is also an increase in the dispersity of platinum (the particle size diminishes from 130 to 60 Å) and there is also a decrease in the fraction of well crystallised platinum. After activation, there is no interaction of the active components with one another and with the carrier and the SnO_2 and Pt phases are present on the carrier surface.

A solid solution of tin in platinum with a face-centred cubic lattice is formed during the dehydrogenation reaction. For the ratios Pt:Sn = 1:3 and 1:5, the intermetallic compound Pt_3Sn with a primitive cubic cell is formed, whereas in the presence of a high platinum content the PtSn and $PtSn_2$ alloys are produced.

An important feature of the catalysts investigated is that the platinum–tin alloys are stable only in the reaction medium and are produced solely when acted upon by the latter. The regeneration of

the catalyst (elimination of carbonaceous deposits) leads to the decomposition of the alloys. However, when a new dehydrogenation cycle is carried out, the platinum–tin alloys are reformed already in the first minutes.

The role of the modifying additive is interesting. The tin in the platinum catalysts deposited on a spinel can play a dual role—it can serve either as a promoting agent, increasing appreciably the activity and selectivity of platinum in the lower paraffin dehydrogenation reaction (alloys containing $\leqslant$25 at.% of tin, having the platinum structure, are then formed in the catalyst) or behaves as a catalytic poison (on formation of alloys with a high tin content). Similar results were obtained for catalysts deposited on a magnesium–aluminium spinel.

3. Nickel–tin catalysts

The addition of tin to aluminonickel catalysts alters significantly the mode of reaction of unsaturated hydrocarbons: nickel catalysts accelerate the hydrogenolysis reaction, while nickel–tin catalysts on γ-Al_2O_3 exhibit an aromatising activity at high temperatures, which is typical of the Pt/Al_2O_3 catalysts.[124]

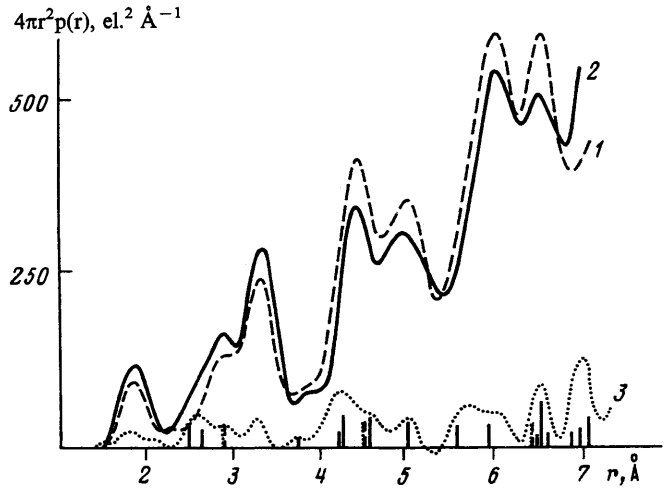


Figure 6. RDA curves for the γ-Al_2O_3 carrier (curve *1*) and the aluminonickel–tin catalyst (curve *2*) as well as the difference RDA curve (curve *3*).[128]

Diffractometric studies[128] of nickel–tin catalysts (1.7 wt.% Ni + 3.5 wt.% Sn on aluminium oxide) showed that the α-Sn phase with a particle size of 50 Å and a metallic nickel phase are formed in the specimens reduced at 823 K. Metallic nickel phases with a face-centred cubic structure (r = 2.50, 4.30, 5.56, and 6.58 Å), metallic α-Sn phases (r = 2.97, 3.17, 4.57, and 6.49 Å), and metallic nickel phases with a hexagonal structure (r = 2.66, 3.75, 4.33, 4.60, 5.08, and 5.93 Å) are detected on the difference RDA curve (Fig. 6). The stabilisation of the last structure is known to require the obligatory presence of admixtures of other metals. Indeed, data concerning the effect of temperature on the relative magnetisation of nickel–tin catalysts show that their Curie point is lower by 40 K than for the catalyst without the additive. This confirms the formation of a nickel–tin alloy (containing 2% of tin). X-Ray spectroscopic data and analysis of the Mössbauer spectra also confirm the presence of a Ni–Sn alloy in the catalysts investigated, but the Mössbauer spectroscopic data indicate also the presence of Sn^{2+} in the carrier structure. The RDA curves also have maxima corresponding to the interatomic distances in the phase in which the tin interacts with aluminium oxide (r = 1.76 and 3.30 Å). The surface Sn^{2+} ions on the carrier are apparently centres for the stabilisation of highly disperse alloy particles.

VI. Conclusion

Thus, despite the apparently small amount of information contained in the initial diffraction data (the diffraction peaks are small, diffuse, and frequently superimposed on another), an appropriate formulation of the experiment with interpretation of the results by modern computer techniques makes it possible to obtain a lot of useful data on the phase composition (RDA method) and the structural (FPA method) and substructural (RDA and MDSC methods) characteristics of the test objects.

During the last decade, the long-range fine structure of the X-ray absorption spectra of a given chemical element (EXAFS spectroscopy) began to be studied widely in the investigation of the structure of its local environment.[46,47] This method has many advantages over the X-ray RDA method: (1) selectivity, associated with the possibility of obtaining independent RDA curves for the local environment of each chemical element in the specimen; (2) the possibility of determining not only the interatomic distances and coordination numbers but also the kind of atoms in the vicinity of the specified atom. A powerful source of X-rays (synchrotron radiation) is usually employed in this method, which makes it highly sensitive and rapid. Such a source can be used also in the X-ray diffraction method. However, the EXAFS method is inferior to the X-ray diffraction RDA method in that the information obtained with its aid concerns mainly 1–2 coordination spheres in the structure, which significantly hinders the analysis of the structural characteristics. On the other hand, one obtains by the EXAFS method interatomic distances which are not absolute but involve a phase shift. Problems arise also in the determination of the coordination numbers.

Despite the existence of a number of difficulties concerning also the very principles of the EXAFS method and the procedures used to extract structural information, at the present time it is widely employed in the study of catalysts.[47] The data for metallic deposited catalysts obtained by this method in the main agree with the results obtained previously by the X-ray diffraction RDA method. It is apparently useful to combine the two methods.

References

1. R M Lambert *Characterisation of Catalysts* (Edited by J M Thomas, R M Lambert) (Translated into Russian), Mir, Moscow, 1983, 294 pp.
2. J R Anderson *Structure of Metallic Catalysts* (Translated into Russian), Mir, Moscow, 1978, p. 398
3. V Valvoda *First European Powder Diffraction Conference: Abstracts*, Münich, 1991, p. 7

4. M Gamarnik *First European Powder Diffraction Conference: Abstracts*, Münich, 1991, p. 38
5. N Mattern *First European Powder Diffraction Conference: Abstracts*, Münich, 1991, p. 41
6. L G Shabelnikov *First European Powder Diffraction Conference: Abstracts*, Münich, 1991, p. 60
7. J F Faudon, G Bergeret, A Renouprez *First European Powder Diffraction Conference: Abstracts*, Münich, 1991, p. 117
8. E M Moroz, V A Ushakov, S V Bogdanov *First European Powder Diffraction Conference: Abstracts*, Münich, 1991, p. 118
9. K Richter, B Peplinski, P Doppler *First European Powder Diffraction Conference: Abstracts*, Münich, 1991, p. 128
10. R F Skryshevskii *Strukturnyi Analiz Zhidkostei i Amorfnykh Tel* (Structural Analysis of Liquids and Amorphous Bodies), Vys. Shkola, Moscow, 1980, 328 pp.
11. A N V Temperley, J S Rowlinson, G S Rushbrooke *Physics of Simple Liquids. Experimental Studies* (Translated into Russian), Mir, Moscow, 1971, 308 pp.
12. Yu G Poltavtsev *Struktura Poluprovodnikovykh Rasplavov* (The Structure of Semiconductor Melts), Metallurgiya, Moscow, 1984, 176 pp.
13. R Mozzi, B E Warren *J. Appl. Crystallogr.*, 1969, **2**(7) 149
14. B K Vainshtein *Kristallografiya*, 1957, **2** 29
15. R Hoseman, S N Bagchi *Direct Analysis of Diffraction by Matter*, Amsterdam, 1962, p. 111
16. Ya I Stetsiv *Kristallografiya*, 1973, **18** 484
17. V G Nagornyi, D K Khakimov, A N Avdeev *Kristallografiya*, 1973, **20** 900
18. F A Brusentsev *Matematicheskie Metody Resheniya Nekotorykh Zadach Fiziki Tverdogo Tela i Strukturnoi Khimii s Ispol'zovaniem ETsVM* (Mathematical Methods for the Solution of Certain Problems in Solid State Physics and Structural Chemistry Using Computers), Naukov Dumka, Kiev, 1973, p. 239
19. J T Randall *Diffraction of X-Rays and Electrons by Amorphous Solids, Liquids and Gases*, London, 1964, 240 pp.
20. E M Moroz, Doctoral Thesis in Chemical Sciences, Institute of Catalysis of the Siberian Division of the USSR Academy of Sciences, Novosibirsk, 1989, 333 pp.
21. L I Tatarinova *Struktura Tverdykh Amorfnykh i Zhidkikh Veshchestv* (The Structure of Solid Amorphous and Liquid Substances), Nauka, Moscow, 1983, p. 151
22. A J Leonard, P N Semaille, J J Fripiat *Proc. British Ceramic Solid*, 1969, **13** 109
23. P Ratnasamy, A J Leonard *Catal. Rev.*, 1972, **6** 293
24. P Ratnasamy, A J Leonard, L Rodrique, J J Fripiat *J. Catal.*, 1973, **29** 374
25. P Ratnasamy, A J Leonard *J. Phys. Chem.*, 1972, **76** 1838
26. P Gallezot, A Bienenstock, M Boudart *Nouv. J. Chim.*, 1978, **2** 263
27. K G Rikhter, Candidate's Thesis in Chemical Sciences, Institute of Catalysis of the Siberian Division of the USSR Academy of Sciences, Novosibirsk, 1973, 144 pp.
28. K G Rikhter, S V Ketchik, L G Simonova, M S Borisova *Kinet. Katal.*, 1975, **16** 1298
29. K G Rikhter, E M Moroz, E A Levitskii, V I Kolomiichuk *Kinet. Katal.*, 1975, **16** 1578
30. N C Halder, R J Metzger, C N Wagner *J. Chem. Phys.*, 1966, **45** 1259
31. D T Keeting *J. Appl. Phys.*, 1963, **34** 923
32. C W Grigson, E Barton *Brit. J. Appl. Phys.*, 1966, **17** 1019
33. C W Grigson, E Barton *Brit. J. Appl. Phys.*, 1967, **18** 175
34. V N Kolomiichuk *Metody Issledovaniya Kataliticheskikh Sistem* (Methods for the Study of Catalytic Systems). Vol. 1. *Rentgenografiya Katalizatorov* (X-Ray Diffraction of Catalysts) (Edited by V N Kolomiichuk), Izd. Inst. Katal. Sib. Otd. Akad. Nauk SSSR, Novosibirsk, 1977, p. 67
35. E M Moroz, S V Bogdanov, V A Ushakov *React. Kinet. Catal. Lett.*, 1978, **9** 109
36. E M Moroz, V A Ushakov, G R Kosmambetova, et al. *Kinet. Katal.*, 1988, **29** 1446
37. E M Moroz, S V Bogdanov, N E Buianova, O S Kovrizhina *Kinet. Katal.*, 1978, **19** 1029
38. E M Moroz, S I Bogdanov, V A Ushakov, E A Levitskii *Kinet. Katal.*, 1979, **20** 173
39. K G Rikhter, E A Levitskii, V N Kolomiichuk, E M Moroz *Kinet. Katal.*, 1975, **16** 1578
40. O N Kimkhai, B N Kuznetsov, N A Pashkovskaya, et al. *React. Kinet. Catal. Lett.*, 1977, **6** 393
41. E M Moroz, A A Tripol'skii, Yu A Ryndin, E N Kuznetsov *Kinet. Katal.*, 1977, **18** 1531
42. E M Moroz, V A Ushakov, S V Bogdanov, V A Gusev *Metody Issledovaniya Kataliticheskikh Sistem* (Methods for the Study of Catalytic Systems). Vol. 1. *Rentgenografiya Katalizatorov* (X-Ray Diffraction of Catalysts) (Edited by V N Kolomiichuk), Izd. Inst. Katal. Sib. Otd. Akad. Nauk SSSR, Novosibirsk, 1977, p. 53
43. H Krebs, H J Gruber *Z. Naturforsch., A*, 1967, **22** 96
44. P E Kolosov *Kataliz v Neftekhimii i Neftepererabotke: Regional'naya Shkola-Seminar Molodykh Uchenykh. Omsk* (Catalysis in Petrochemistry and Petroleum Processing: Regional School-Seminar for Young Scientists. Omsk), Omsk, 1990, p. 91
45. P E Kolosov, E M Moroz *Kinet. Katal.* (in the press)
46. D I Kochubei *Usp. Khim.*, 1986, **55**(3) 418 [English translation in *Russ. Chem. Rev.*, 1986(3)]
47. D I Kochubei, Yu A Babanov, K I Zamaraev, et al. *Rentgenospektral'nyi Metod Izucheniya Struktury Amorfnykh Tel: EXAFS-Spektroskopiya* (X-Ray Spectroscopic Method for the Study of the Structures of Amorphous Susbtances: EXAFS Spectroscopy), Nauka, Novosibirsk, 1988, 306 pp.
48. H M Rietveld *J. Appl. Crystallogr.*, 1969, **2** 65
49. R A Young, P E Mackie, R B von Dreel *J. Appl. Crystallogr.*, 1977, **10** 262
50. C P Khatak, D E Cox *J. Appl. Crystallogr.*, 1977, **10** 405
51. L D Calvert, E J Gobe, Y Page *Acta Crystallogr.*, 1981, **37** 314
52. R A Young, D B Wiles *Adv. X-Ray Analysis*, 1981, **24** 1
53. S D Kirik, S V Borisov, V G Fedorov *Zh. Strukt. Khim.*, 1981, **22**(2) 130
54. S D Kirik, I S Yakimov *Trudy Instituta Tsvetnykh Metallov* (Transactions of the Institute of Non-ferrous Metals), Krasnoyarsk, 1985, p. 20
55. C Clark, D K Smith, G G Jonson *Bull. Exper. Stat. Pensylvania*, 1973
56. A Albinati, B T Willis *J. Appl. Crystallogr.*, 1982, **15** 361
57. G S Pawley *J. Appl. Crystallogr.*, 1980, **13** 630
58. S V Tsybulya, L P Solov'eva *Apparatura i Metody Rentgenovskogo Analiza* (Apparatus and Methods for X-Ray Analysis), Leningrad, 1988, No. 38, p. 46

59. L P Solov'eva, S V Tsybulya, V A Zabolotnyi *Trudy Seminara "Rentgenostrukturnyi Analiz Polikristallov". Rostov-na-Donu* (Proceedings of the Seminar on "X-Ray Diffraction Analysis of Polycrystalline Materials". Rostov-on-don), Izd. Kalmytskogo Univ., Rostov-on-Don, 1986, p. 81
60. C J Howard *J. Appl. Crystallogr.*, 1982, **15** 615
61. A Brown, J M Edmonds *Adv. X-Ray Analysis*, 1980, **23** 361
62. V A Kogan, M F Kupriyanov, E G Fesenko *Kristallografiya*, 1988, **33** 1368
63. V A Kogan, M F Kupriyanov *First European Powder Diffraction Conference. Abstracts*, Münich, 1991, p. 16
64. G Caglioti, A Paoletti, F P Ricci *Nucl. Instrum.*, 1958, **3** 223
65. A N Hewat *J. Phys. Chem.*, 1973, **6** 2559
66. B W Lucas *Acta Crystallogr., Sect. B*, 1979, **35** 1038
67. B Moraveck, P Montgolfier, A J Renouprez *J. Appl. Crystallogr.*, 1977, **10** 184
68. A Glazer, S Mabud *Acta Crystallogr.*, 1978, **34** 1060
69. V A Ushakov, E M Moroz *Kinet. Katal.*, 1985, **26** 968
70. H Bosman *Acta Crystallogr.*, 1970, **26** 649
71. G Burchard, W Rudolff *Z. Anorg. Allg. Chem.*, 1978, **445** 79
72. A Mangeli *Reactiv. Solids. Proc. 8th Intern. Symp. Göteborg*, 1976, New York, 1977, p. 1
73. L P Solov'eva, S V Tsybulya, I P Olen'kova, L N Plyasova *Zh. Strukt. Khim.*, 1984, **25**(5) 177
74. I V Smushkov, V F Tkachenko *Monokristally, Stsintillyatory i Organicheskie Lyuminofory* (Single Crystals, Scintillators, and Organic Phosphors), Izd. Kharkov. Gos. Univ., Kharkov, 1967, No. 2, p. 43
75. E M Moroz, Candidate's Thesis in Physical-Mathematical Sciences, Institute of Catalysis of the Siberian Divison of the USSR Academy of Sciences, Novosibirsk, 1971, 146 pp.
76. V I Iveronova, G P Revkevich *Teoriya Rasseyaniya Rentgenovskikh Luchei* (Theory of X-Ray Scattering), Izd. Moskov. Gos. Univ., Moscow, 1978, p. 129
77. B E Warren *Advances in Metal Physics* (Translated into Russian), Metallurgizdat, Moscow, 1963, Vol. 5, p. 172
78. A Guinier *X-Ray Diffraction of Crystals* (Translated into Russian), Fizmatgiz, Moscow, 1961, 392 pp.
79. E Bertaut *Acta Crystallogr.*, 1950, **3** 14
80. H Spindler, P Orban, B Westphal *Kristalle und Technik*, 1977, **17** 517
81. E M Moroz, S V Bogdanov, et al. *Kinet. Katal.*, 1984, **25** 171
82. S V Bogdanov, E M Moroz, S V Tsybulya *Kinet. Katal.*, 1984, **25** 1203
83. S V Bogdanov, E M Moroz, P G Tsyrul'nikov, et al. *Kinet. Katal.*, 1988, **29** 498
84. B C Lippens, J J Steggerda *The Structure and Properties of Adsorbents and Catalysts* (Translated into Russian), Mir, Moscow, 1973, 190 pp.
85. B C Gates, J R Kutzer, G C A Schuit *Chemistry of Catalytic Processes* (Translated into Russian), Mir, Moscow, 1981, 307 pp.
86. C A Spitler, S S Pollack *J. Catal.*, 1981, **69** 241
87. H P Rooksby *X-Ray Methods for the Study of Argillaceous Minerals and Their Structures* (Translated into Russian), Mir, Moscow, 1965, 405 pp.
88. S Yamaguchi *Z. Anal. Chem.*, 1974, **270** 191
89. A J Leonard, D Semaile, J J Fripiat *Proc. Brit. Ceram. Soc.*, 1969, **13** 103
90. E M Moroz, T D Kambarova *Metody Issledovaniya Kataliticheskikh Sistem* (Methods for the Study of Catalytic Systems). Vol. 1. *Rentgenografiya Katalizatorov* (X-Ray Diffraction of Catalysts) (Edited by V N Kolomiichuk), Izd. Inst. Katal. Sib. Otd. Akad. Nauk SSSR, Novosibirsk, 1977, p. 110
91. R A Shkrabina, Yu K Vorob'ev, E M Moroz, et al. *Kinet. Katal.*, 1981, **22** 1080
92. Yu K Vorob'ev, R A Shkrabina, E M Moroz, et al. *Kinet. Katal.*, 1981, **22** 1595
93. V A Ushakov, E M Moroz *Kinet. Katal.*, 1985, **26** 963
94. V A Ushakov, E M Moroz *Kinet. Katal.*, 1985, **26** 1200
95. E M Moroz, V A Ushakov, S B Bogdanov *15th Congress and General Assembly of International Union of Crystallography. Collected Abstracts.* Bordeau (France), 1990, p. 371
96. V A Ushakov, E M Moroz *React. Kinet. Catal. Lett.*, 1984, **24** 113
97. G B Erenburg, V P Fateeva, A I Min'kov, et al. *Izv. Sib. Otd. Akad. Nauk SSSR, Ser. Khim.*, 1981, **1**(2) 54
98. S Soled *J. Catal.*, 1983, **81** 252
99. D Espinat, F Thevenot, K Malkio *12th European Crystallographic Meeting. Abstracts*, Moscow, 1989, Vol. 3, p. 280
100. V N Kuklina, E A Levitskii, E M Plyasova, et al. *Kinet. Katal.*, 1972, **13** 1269
101. A S Ivanova, V A Dzis'ko, E M Moroz, et al. *Kinet. Katal.*, 1985, **26** 429
102. E M Moroz, V N Kuklina, V A Ushakov *Kinet. Katal.*, 1987, **28** 699
103. V A Dzis'ko, A S Ivanova, L M Plyasova, S V Ketchik *Izv. Akad. Nauk SSSR, Ser. Khim.*, 1978, 983
104. E M Moroz, O A Kirichenko, V A Ushakov, E A Levitski *React. Kinet. Catal. Lett.*, 1985, **28** 9
105. R A Shkrabina, E M Moroz, E A Levitskii *Kinet. Katal.*, 1981, **22** 1293
106. T F Limar', Yu A Kagan, L A Shepelenko, N T Kisel' *Izv. Akad. Nauk SSSR, Neorg. Mater.*, 1972, **8** 500
107. S V Tsybulya, L P Solov'eva, G N Kryukova, E M Moroz *Zh. Strukt. Khim.*, 1991, **32**(3) 18
108. L Lutterotti, P Scardi *J. Appl. Crystallogr.*, 1990, **23** 246
109. Yu I Yermakov, V F Surovikin, G V Plaksin, et al. *React. Kinet. Catal. Lett.*, 1987, **33** 435
110. V L Kuznetsov, M N Aleksandrov, I V Zagoruiko, et al. *Carbon*, 1991, **29** 665
111. P A Simonov, E M Moroz, V A Likholobov, G V Plaksin *Izv. Akad. Nauk SSSR, Ser. Khim.*, 1990, 1478
112. E M Moroz, S D Mikhailenko, A K Dzhunusov, A B Fasman *React. Kinet. Catal. Lett.*, 1991, **43** 63
113. N E Buyanova, O F Zapreeva, A P Karnaukhov, et al. *Kinet. Katal.*, 1977, **18** 736
114. V A Ushakov, E M Moroz, K G Rikhter, et al. *Dokl. Akad. Nauk SSSR*, 1974, **219** 158
115. V A Ushakov, E M Moroz, P A Zhdan, et al. *Kinet. Katal.*, 1978, **19** 744
116. V A Ushakov, E M Moroz *React. Kinet. Catal. Lett.*, 1985, **27** 351
117. E M Moroz, S D Mikhailenko, A K Dzhunusov, et al. *Kinet. Katal.*, 1990, **31** 1506

118. Yu I Ermakov *Nanesennye Metallicheskie Katalizatory Prevrashcheniya Uglevodorodov* (Deposited Metallic Catalysts of the Reactions of Hydrocarbons), Izd. Inst. Kataliza Sib. Otd. Akad. Nauk SSSR, Novosibirsk, 1978, Part 1, p. 90
119. M D Smolikov, A S Belyi, A Nizovskii, et al. *React. Kinet. Catal. Lett.*, 1988, **37** 437
120. A S Belyi, M D Smolikov, N M Ostrovskii, V K Duplyakin *React. Kinet. Catal. Lett.*, 1988, **37** 457
121. V A Ushakov, E M Moroz, N R Bursian, et al. *Kinet. Katal.*, 1979, **20** 177
122. A N Startsev, T M Moravskaya, B N Kuznetsov, et al. *Nanesennye Metallicheskie Katalizatory Prevrashcheniya Uglevodorodov* (Deposited Metallic Catalysts of the Reactions of Hydrocarbons), Izd. Inst. Kataliza Sib. Otd. Akad. Nauk SSSR, Novosibirsk, 1978, Part 2, p. 157
123. Yu I Ermakov, B N Kuznetsov, A N Startsev *Nanesennye Metallicheskie Katalizatory Prevrashcheniya Uglevodorodov* (Deposited Metallic Catalysts of the Reactions of Hydrocarbons), Izd. Inst. Kataliza Sib. Otd. Akad. Nauk SSSR, Novosibirsk, 1978, Part 2, p. 195
124. Yu A Ryndin, E M Moroz, B N Kuznetsov, et al. *Nanesennye Metallicheskie Katalizatory Prevrashcheniya Uglevodorodov* (Deposited Metallic Catalysts of the Reactions of Hydrocarbons), Izd. Inst. Kataliza Sib. Otd. Akad. Nauk SSSR, Novosibirsk, 1978, Part 2, p. 239
125. V K Duplyakin *Nanesennye Metallicheskie Katalizatory Prevrashcheniya Uglevodorodov* (Deposited Metallic Catalysts of the Reactions of Hydrocarbons), Izd. Inst. Kataliza Sib. Otd. Akad. Nauk SSSR, Novosibirsk, 1978, Part 1, p. 74
126. B N Kuznetsov, A N Startsev, V K Duplyakin *Nanesennye Metallicheskie Katalizatory Prevrashcheniya Uglevodorodov* (Deposited Metallic Catalysts of the Reactions of Hydrocarbons), Izd. Inst. Kataliza Sib. Otd. Akad. Nauk SSSR, Novosibirsk, 1978, Part 2, p. 43
127. N A Pakhomov, R A Buyanov, G R Kotel'nikov, et al. *VII Sovetsko-Yaponskii Seminar po Katalizu: Doklady. Irkutsk* (The VIIth Soviet-Japanese Seminar on Catalysis: Reports. Irkutsk), Irkutsk, 1983, p. 172
128. E M Moroz, B N Kuznetsov, A N Startsev, et al. *Nanesennye Metallicheskie Katalizatory Prevrashcheniya Uglevodorodov* (Deposited Metallic Catalysts of the Reactions of Hydrocarbons), Izd. Inst. Kataliza, Sib. Otd. Akad. Nauk SSSR, Novosibirsk, 1978, Part 2, p. 219
129. E M Moroz *Fizikokhimiya Ul'tradispersnykh Sistem* (Physical Chemistry of Ultradisperse Systems), Nauka, Moscow, 1987, p. 85